Available online at www.sciencedirect.com
SCIENCE DIRECT®
Journal of Sound and Vibration 290 (2006) 1040–1070
JOURNAL OF SOUND AND VIBRATION
www.elsevier.com/locate/jsvi

Dynamic behavior comparison of passive hydraulic engine mounts. Part 1: Mathematical analysis

J. Christopherson, G. Nakhaie Jazar*

Department of Mechanical Engineering and Applied Mechanics, North Dakota State University, Fargo, ND 58105, USA

Received 4 October 2004; received in revised form 20 April 2005; accepted 6 May 2005
Available online 10 August 2005

Abstract

This paper investigates the linear and nonlinear modeling aspects of two distinct types of passive hydraulic engine mounts. The two mounts considered here within differ by the means in which the decoupler is used to control the amplitude-dependent behavior of the hydraulic mount. Both of the mounts decoupler action introduces nonlinearities into the system; however, one mount illustrates parametric-type behavior. Because one mount exhibits parametric behavior the energy-rate method is used to determine the stability of the system. The linear and nonlinear models are directly compared with each other in a frequency domain for each respective mount, and then the nonlinear models are compared directly against each other to ascertain a comparison between mount designs, again in a frequency domain.

1. Introduction

Hydraulic mounts have been used in the automotive industry since the mid-1980s as a means to provide an adaptive vibration isolation system to meet increasing customer demand for quieter and smoother riding vehicles [1]. More specifically, the hydraulic mount was introduced to provide a dual damping mode passive vibration isolator to control high-amplitude, low-frequency road-induced vibrations and low-amplitude, high-frequency engine-induced vibrations [2]. The hydraulic mount meets the requirements for a dual damping mode isolator by use of a device

*Corresponding author. Tel.: +1 701 231 8303; fax: +1 701 231 8913.
E-mail address: reza.n.jazar@ndsu.edu (G.N. Jazar).

0022-460X/$ - see front matter © 2005 Elsevier Ltd. All rights reserved.
doi:10.1016/j.jsv.2005.05.008

Nomenclature

A	cross-sectional area
A_B	decoupler disk piston area
A_p	equivalent piston area
B_r	equivalent rubber damping coefficient
B	equivalent viscous damping coefficient
M	effective fluid column mass
K_r	upper structure stiffness
C	volumetric compliance
K	sum of inverse compliance
P	fluid chamber pressure
Q	volumetric flow rate
f_T	transmitted force
F_T	amplitude of transmitted force
K_{dyn}	dynamic stiffness
ϕ	phase lag
r	nondimensional amplitude
R	dimensional amplitude
X	excitation amplitude
ω	excitation frequency
t	time
E	nonlinear coefficient
Δ	decoupler gap size
s	Laplace transformation variable
j	complex variable
Ψ	any integer
U	energy
T	period of oscillation

Subscripts

i	inertia track
d	decoupler
fd	floating-decoupler
dd	direct-decoupler
dyn	dynamic
sys	system
atm	atmospheric
1,2,3	fluid control volume number

referred to as the decoupler in conjunction with a passage known as the inertia track. In its most common form the hydraulic mount is as illustrated in Fig. 1, and consists of two fluid-filled chambers separated by a metallic plate containing the decoupler and inertia track. The decoupler is simply a disk that floats in the cage provided by the metallic plate, and acts as a mechanical switch to either allow fluid through or block fluid dependent upon the amplitude of excitation [3].

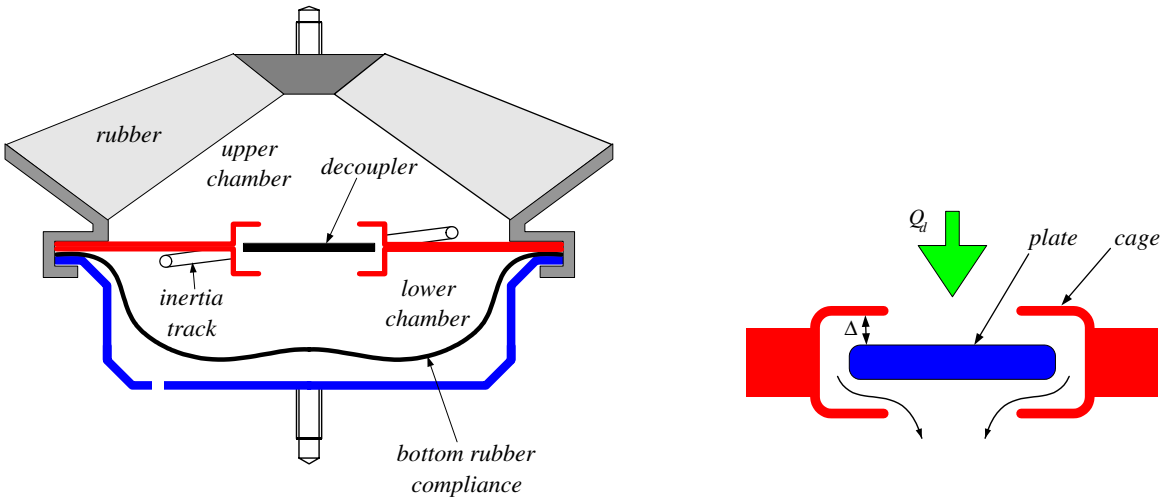

Fig. 1. Illustration of a floating-decoupler-type hydraulic mount.

If the decoupler is closed the fluid is forced to flow through the inertia track due to the relative motion of the system (motion of the engine and the motion of the vehicle structure), and when the fluid is forced through the inertia track the overall damping coefficient of the mount increases due to the highly restricted fluid motion through the channel. However, if the decoupler remains open the fluid motion between chambers is relatively unrestricted; therefore, the overall damping of the mount decreases. Hence, this design of engine mount relies upon determining the appropriate combination of inertia track size and decoupler gap size (see Fig. 1) to control the mount behavior [4].

An alternative to the aforementioned hydraulic mount is illustrated in Fig. 2 and fixes the decoupler directly to the engine side of the mount; therefore, the decoupler motion is controlled directly by the input excitation provided by the engine and vehicle structure. To accommodate the decoupler in this type mount an extra fluid chamber is introduced and it is from this chamber that the inertia track exits (see Fig. 2). This additional fluid chamber, labeled the middle chamber, provides a means by which to ensure activity of the inertia track, as opposed to relying on fluid pressure differentials to close the decoupler, to provide additional damping from the inertia track. Therefore, the overall damping of this type of mount is less sensitive to decoupler gap size; however, the mount becomes increasingly dependent upon the inertia track geometry. This is not to say that the decoupler gap size and geometry are unimportant, quite the contrary; however, the inertia track is more prevalent as compared with the previous design. In addition, the decoupler does provide additional damping to the system when it approaches its cage bounds noting that as the decoupler moves it forces fluid out and around it (see Fig. 2); therefore, as the decoupler approaches the cage bounds the fluid resistance associated with it changes as a function of the decoupler position. This motion provides additional damping and increased nonlinearity to this type of mount.

This paper is the first of a two part series describing the mathematical modeling and finite element modeling and results for the two distinct types of passive hydraulic engine mounts

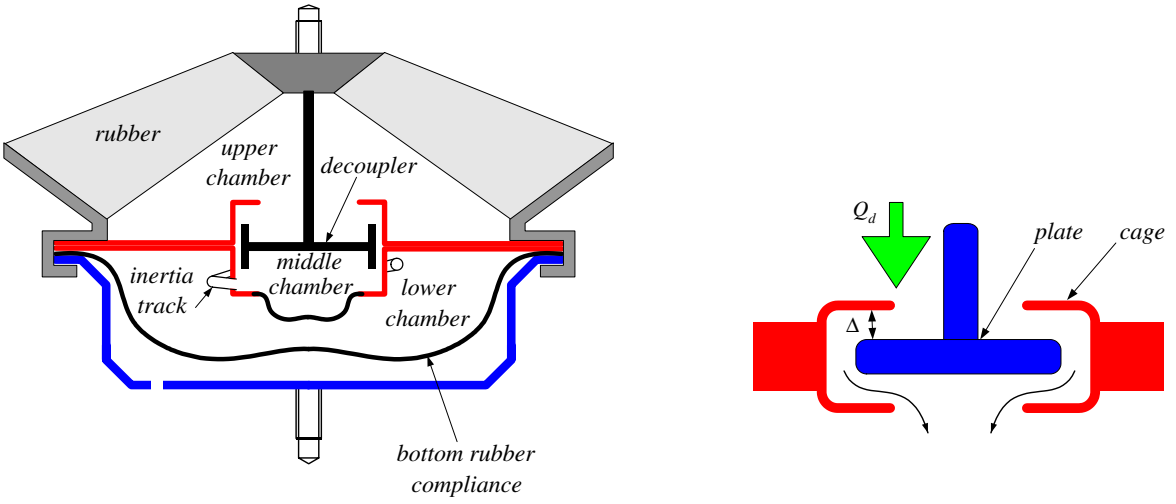

Fig. 2. Illustration of a direct-decoupler-type hydraulic mount.

previously discussed. As stated the engine mounts considered in this series utilize two different means of controlling the amplitude-sensitive behavior of the hydraulic mount. The standard method of controlling the amplitude-sensitive behavior is through the device of a mechanical switching device introduced as the floating-decoupler (see Fig. 1). An alternative method is to directly fix the decoupler to the input of the engine mount (see Fig. 2) thereby directly controlling the decoupler motion. Both of the aforementioned mounts are currently used in automotive applications and models of each mount may be seen in Figs. 3 and 4.

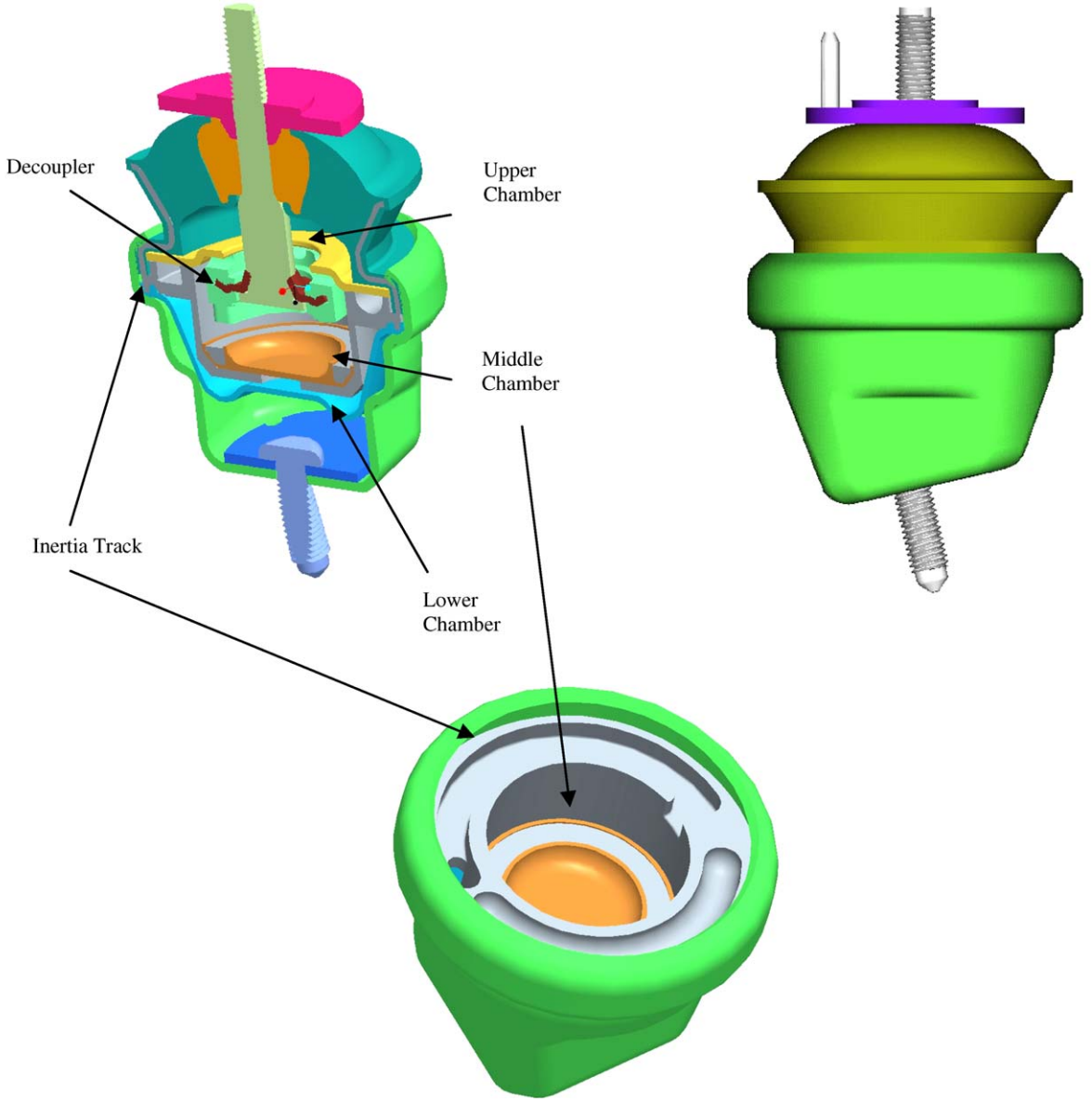

Fig. 3. Direct-decoupler hydraulic mount.

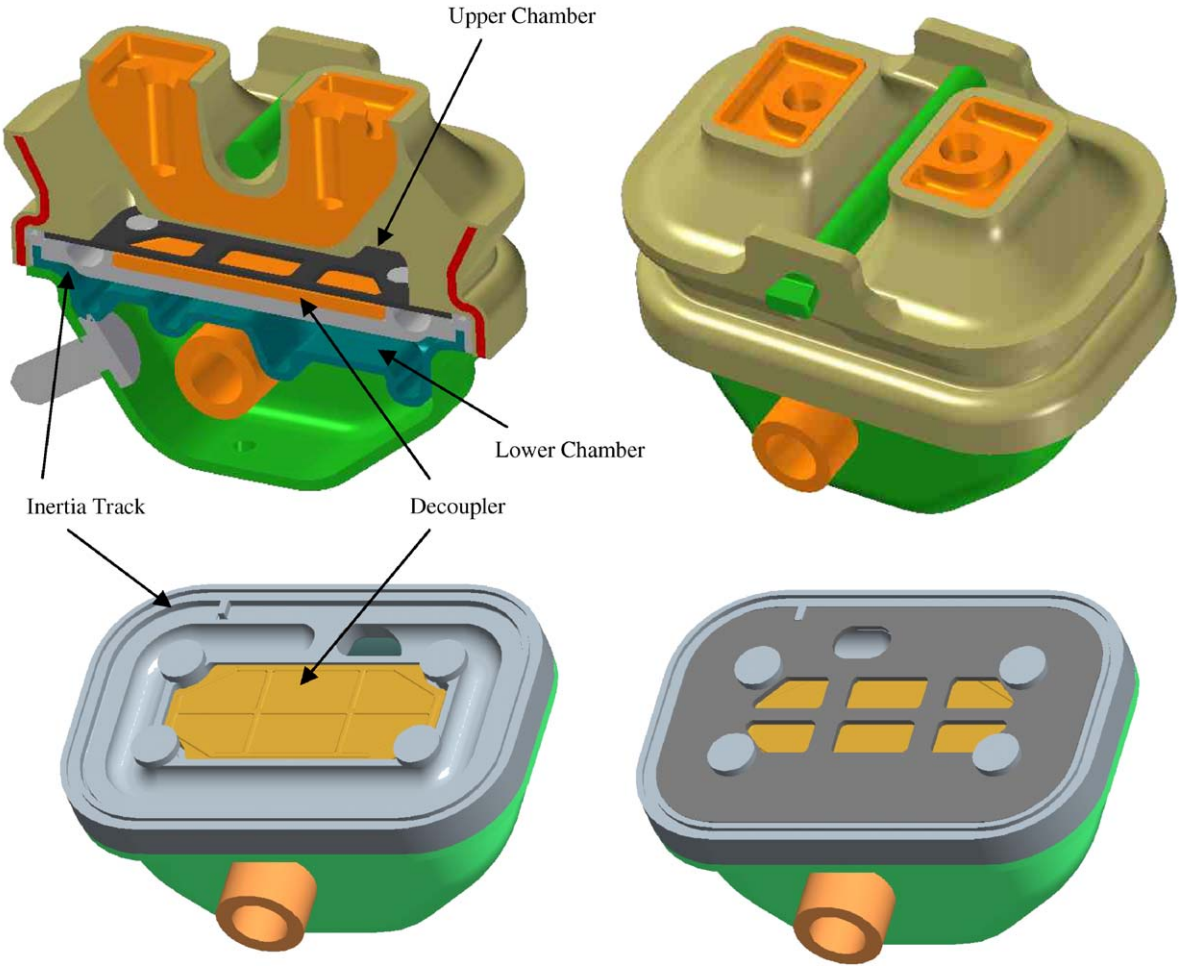

Fig. 4. Floating-decoupler hydraulic mount.

The passive hydraulic mount has been thoroughly studied by many researchers; however, to date the decoupler dynamics present several modeling difficulties. Flower was the first to analyze the dynamic behavior of the hydraulic mount through the use of linear models in which the decoupler was either always open or always closed [1]. Singh et al. [5] and Kim and Singh [6] have illustrated the applicability of such modeling techniques for limited frequency domains thereby introducing the limitation of the linear modeling techniques in that they never consider the true decoupler switching mechanism. To remedy this piecewise linear models are considered in which the decoupler is treated as open until the decoupler disk itself reaches the cage bounds which it then is modeled as being completely closed [3]. The disadvantage of such modeling techniques is they are discontinuous in nature and provide large nonlinearities which can be difficult to deal with mathematically. To this end several researchers have used various nonlinear models in which the decoupler behavior is considered as a continuous function and the possibility for leak flow

through the decoupler when closed is allowed [2,6–8]. Of the nonlinear models, the simplest model uses a cubic nonlinear function to alter the resistance to fluid flow through the decoupler [7,8]. In addition to considering decoupler nonlinearities Geisberger et al. [2] and Adiguna et al. [9] have used experimental approaches to determine not only the decoupler flow characteristics, but also the inertia track flow characteristics. Adiguna et al. [9] have also experimentally shown the possibility of vacuum formation within the hydraulic mount as a source for further nonlinearities. Some recent research has been devoted to finding methods by which to optimize the design of the passive-type hydraulic mount by way of using some of the aforementioned nonlinear modeling techniques. Christopherson and Jazar [4] have proposed and illustrated an optimization routine based on a rms averaging of the frequency domain behavior of the hydraulic mount that converges to provide real results [4]. In addition to the analytical modeling approaches utilized by the aforementioned researchers Shannggguan and Lu [10] have illustrated the applicability of nonlinear finite elements in conjunction with fluid–structure interaction to the analysis of hydraulic mounts for use as yet another design tool.

However, in all the aforementioned research no one to the authors' knowledge has published significant information regarding direct-decoupler-type passive hydraulic engine mount designs as illustrated in Figs. 2 and 3 even though such designs are being used in modern automotive applications. This series of papers addresses the modeling of one such design of an alternative passive hydraulic mount design even though other passive hydraulic mount designs do exist, this paper limits itself to a comparison between the two designs previously discussed.

2. Mathematical model

2.1. Linear models

Linear models are first developed to describe the frequency domain behavior of both hydraulic mounts. These models neglect the decoupler closing action for either mount considering the decoupler an open path. Figs. 5 and 6 illustrate the lumped parameter models utilized to describe the floating-decoupler and direct-decoupler-type mounts.

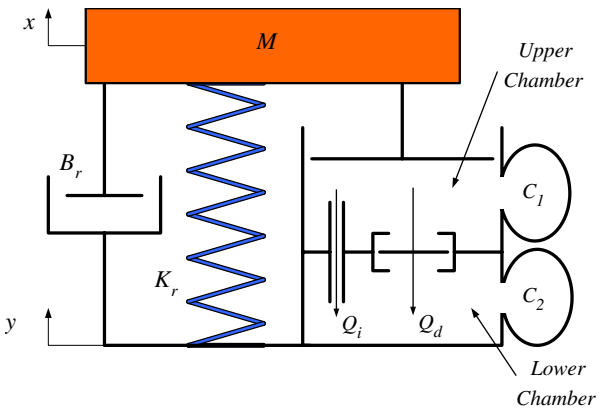

Fig. 5. Lumped parameter model (floating-decoupler).

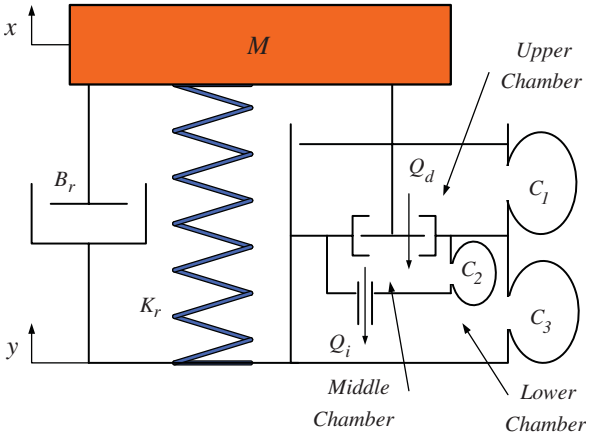

Fig. 6. Lumped parameter model (direct-decoupler).

2.1.1. Floating-decoupler mount

Considering the lumped parameter model illustrated in Fig. 5 as two separate control volumes and allowing the flow through the inertia track and decoupler to be modeled with a constant velocity field across the cross-section of the channel (plug flow) the flow rate equations for the decoupler and inertia track may be written as follows:

$$Q_d = A_d \dot{x}_d, \tag{1}$$

$$Q_i = A_i \dot{x}_i. \tag{2}$$

Again considering the two control volumes illustrated in Fig. 5 the conservation of momentum and fluid continuity equations may be written as follows:

$$M_d \ddot{x}_d + B_d \dot{x}_d = A_d(P_1 - P_2), \tag{3}$$

$$M_i \ddot{x}_i + B_i \dot{x}_i = A_i(P_1 - P_2), \tag{4}$$

$$A_P \dot{x} = Q_d + Q_i + C_1\left(\dot{P}_1 - \dot{P}_{\text{atm}}\right), \tag{5}$$

$$Q_d + Q_i = C_2\left(\dot{P}_2 - \dot{P}_{\text{atm}}\right). \tag{6}$$

Eqs. (1)–(6) fully define the linear model of the floating-decoupler engine mount assuming the decoupler is constantly open. By combining the aforementioned equations and noting that atmospheric pressure is approximately constant over time the following system of second order ordinary equations are realized:

$$\begin{bmatrix} M_d & 0 \\ 0 & M_i \end{bmatrix} \begin{Bmatrix} \ddot{x}_d \\ \ddot{x}_i \end{Bmatrix} + \begin{bmatrix} B_d & 0 \\ 0 & B_i \end{bmatrix} \begin{Bmatrix} \dot{x}_d \\ \dot{x}_i \end{Bmatrix} + \begin{bmatrix} A_d^2 K & A_d A_i K \\ A_d A_i K & A_i^2 K \end{bmatrix} \begin{Bmatrix} x_d \\ x_i \end{Bmatrix} = \frac{A_p}{C_1} \begin{Bmatrix} A_d \\ A_i \end{Bmatrix} x, \tag{7}$$

where

$$K = \frac{C_1 + C_2}{C_1 C_2}, \quad x = X \sin(\omega t).$$

To obtain a solution to Eq. (7) the following Laplace transformation will be introduced:

$$\left(s^2 \begin{bmatrix} M_d & 0 \\ 0 & M_i \end{bmatrix} + s \begin{bmatrix} B_d & 0 \\ 0 & B_i \end{bmatrix} + \begin{bmatrix} A_d^2 K & A_d A_i K \\ A_d A_i K & A_i^2 K \end{bmatrix} \right) \begin{Bmatrix} X_d(s) \\ X_i(s) \end{Bmatrix} = \frac{A_p}{C_1} \begin{Bmatrix} A_d \\ A_i \end{Bmatrix} X(s). \tag{8}$$

Solving Eq. (8) yields the desired frequency domain solutions for the amplitude of the decoupler and inertia track fluid column positions by allowing $s = \mathrm{j}\omega$. Therefore, the solutions obtained by Eq. (8) (see Appendix A) may be expressed in compact notation as follows:

$$\begin{Bmatrix} X_d(\mathrm{j}\omega) \\ X_i(\mathrm{j}\omega) \end{Bmatrix} = \begin{Bmatrix} z_d(\omega) \\ z_i(\omega) \end{Bmatrix} + \mathrm{j} \begin{Bmatrix} Z_d(\omega) \\ Z_i(\omega) \end{Bmatrix}. \tag{9}$$

Using Fig. 5, an equation may be developed by applying Newton's second law to the hydraulic mount to determine the force transmitted as follows:

$$F_T = K_r X(\mathrm{j}\omega) + \mathrm{j}\omega B_r X(\mathrm{j}\omega) + A_p P_1(\mathrm{j}\omega). \tag{10}$$

Using Eq. (9) in conjunction with the continuity equation expressed in Eq. (5), Eq. (10) may be written as follows:

$$F_T = \frac{K_r C_1 X + A_p\left(A_p X - A_d z_d - A_i z_i\right)}{C_1} + \mathrm{j}\left(B_r \omega X - \frac{A_p(A_i Z_i + A_d Z_d)}{C_1} \right). \tag{11}$$

By knowing the transmitted force as expressed in Eq. (11) the dynamic stiffness may be expressed in a real frequency domain by considering the magnitude of the complex function. The phase lag of the system may also be considered by computing the angle of the complex function as follows:

$$K_{\mathrm{dyn}} = \left| \frac{F_T}{X} \right| = \sqrt{\left(\frac{K_r C_1 X + A_p\left(A_p X - A_d z_d - A_i z_i\right)}{C_1 X} \right)^2 + \left(B_r \omega - \frac{A_p(A_i Z_i + A_d Z_d)}{C_1 X} \right)^2}, \tag{12}$$

$$\phi_{\mathrm{sys}} = \arctan\left(\frac{B_r X \omega - A_p(A_i Z_i + A_d Z_d)}{K_r C_1 X + A_p\left(A_p X - A_d z_d - A_i z_i\right)} \right). \tag{13}$$

2.1.2. Direct-decoupler mount

As with the floating-decoupler mount, the direct-decoupler mount will be analyzed using the lumped parameter approach illustrated in Fig. 6. There are two significant differences between the two mounts. First, the direct attachment of the decoupler to the input of the engine mount, hence the name, and then the inclusion of a third control volume (labeled as the middle chamber) to allow motion of the decoupler. Regardless of the differences between the two mounts the process for analysis is similar. First, the flow rate through both the decoupler and

inertia track is considered.

$$Q_d = A_d \dot{x}_d, \tag{14}$$

$$Q_i = A_i \dot{x}_i. \tag{15}$$

Next, the fluid momentum and continuity equations may be written based upon the lumped parameter model illustrated in Fig. 6 as follows:

$$M_d \ddot{x}_d + B_d \dot{x}_d = A_d(P_1 - P_2), \tag{16}$$

$$M_i \ddot{x}_i + B_i \dot{x}_i = A_i(P_2 - P_3), \tag{17}$$

$$(A_p - A_B)\dot{x} = Q_d + C_1(\dot{P}_1 - \dot{P}_{\text{atm}}), \tag{18}$$

$$Q_d + A_B \dot{x} = Q_i + C_2(\dot{P}_2 - \dot{P}_3), \tag{19}$$

$$Q_i + C_2(\dot{P}_2 - \dot{P}_3) = C_3(\dot{P}_3 - \dot{P}_{\text{atm}}). \tag{20}$$

Using Eqs. (14)–(20) the system of governing linear ordinary equations are written as follows:

$$\begin{bmatrix} M_d & 0 \\ 0 & M_i \end{bmatrix} \begin{Bmatrix} \ddot{x}_d \\ \ddot{x}_i \end{Bmatrix} + \begin{bmatrix} B_d & 0 \\ 0 & B_i \end{bmatrix} \begin{Bmatrix} \dot{x}_d \\ \dot{x}_i \end{Bmatrix} + \begin{bmatrix} A_d^2 K & -\dfrac{A_d A_i}{C_2} \\ -\dfrac{A_d A_i}{C_2} & \dfrac{A_i^2}{C_2} \end{bmatrix} \begin{Bmatrix} x_d \\ x_i \end{Bmatrix} = \begin{Bmatrix} A_d\left(\dfrac{A_p}{C_1} - A_B K\right) \\ \dfrac{A_i A_B}{C_2} \end{Bmatrix} x, \tag{21}$$

where

$$K = \frac{1}{C_1} + \frac{1}{C_2} + \frac{1}{C_3}, \quad x = X \sin(\omega t). \tag{22}$$

As with the floating-decoupler mount, a Laplace transformation will be introduced to solve Eq. (21) for the frequency response functions as

$$\left(s^2 \begin{bmatrix} M_d & 0 \\ 0 & M_i \end{bmatrix} + s \begin{bmatrix} B_d & 0 \\ 0 & B_i \end{bmatrix} + \begin{bmatrix} A_d^2 K & -\dfrac{A_d A_i}{C_2} \\ -\dfrac{A_d A_i}{C_2} & \dfrac{A_i^2}{C_2} \end{bmatrix} \right) \begin{Bmatrix} X_d(s) \\ X_i(s) \end{Bmatrix} = \begin{Bmatrix} A_d\left(\dfrac{A_p}{C_1} - A_B K\right) \\ \dfrac{A_i A_B}{C_2} \end{Bmatrix} X(s). \tag{23}$$

Solving Eq. (23) yields the desired frequency domain solutions for the amplitude of the decoupler and inertia track fluid column positions by allowing $s = \mathrm{j}\omega$. Therefore, the solutions obtained by Eq. (23) (see Appendix A) may be expressed in compact notation as follows:

$$\begin{Bmatrix} X_d(\mathrm{j}\omega) \\ X_i(\mathrm{j}\omega) \end{Bmatrix} = \begin{Bmatrix} z_d(\omega) \\ z_i(\omega) \end{Bmatrix} + \mathrm{j} \begin{Bmatrix} Z_d(\omega) \\ Z_i(\omega) \end{Bmatrix}. \tag{24}$$

Again by the use of Newton's second law and the lumped parameter model (Fig. 6), the transmitted force equation may be written as follows:

$$F_T = K_r X(\mathrm{j}\omega) + \mathrm{j}\omega B_r X(\mathrm{j}\omega) + A_p P_1(\mathrm{j}\omega) + A_B(P_2(\mathrm{j}\omega) - P_1(\mathrm{j}\omega)). \tag{25}$$

Separating Eq. (25) into real and imaginary components the transmitted force equation may be written as follows:

$$F_T = f_T + \mathrm{j}g_T, \tag{26}$$

where

$$f_T = \left(K_r + A_B^2 K + \frac{A_p}{C_1}(A_p - 2A_B)\right)X + A_d\left(A_B K - \frac{A_p}{C_1}\right)z_d - \frac{A_B A_i}{C_2} z_i,$$

$$g_T = B_r X\omega^2 + A_d\left(A_B K - \frac{A_p}{C_1}\right)Z_d - \frac{A_B A_i}{C_2} Z_i.$$

Then by use of Eq. (26) the dynamic stiffness and phase angle equations may be written as follows:

$$K_{\mathrm{dyn}} = \left|\frac{F_T}{X}\right| = \sqrt{\left(\frac{f_T}{X}\right)^2 + \left(\frac{g_T}{X}\right)^2}, \tag{27}$$

$$\phi = \arctan\left(\frac{g_T}{f_T}\right). \tag{28}$$

2.2. Nonlinear models

The nonlinear equations of motion are developed in essentially the same manner for both mounts as the linear model. The difficulty and novelty of the nonlinear model for either mount is describing the decoupler closing event. In the floating-decoupler mount the pressure difference between chambers forces closing and opening of the decoupler; however, in the direct-decoupler mount the decoupler action is directly controlled by the input. Several nonlinear models have been utilized by many researchers [2,6–8] in addition to others using piecewise linear models to describe decoupler behavior [3]. However, the simplest, yet effective, nonlinear model in the literature is the model proposed by Jazar and Golnaraghi to model the decoupler with a function which changes the resistance to fluid flow through the decoupler by noting position and velocity of the fluid within the decoupler [7,8]. This model also allows existence of the leak flow phenomenon described by Singh et al. [6].

$$F_{\mathrm{fd}} = E\frac{x_d^2}{\Delta^2}\dot{x}_d, \tag{29}$$

$$F_{\mathrm{dd}} = E\frac{x^2}{\Delta^2}\dot{x}_d. \tag{30}$$

Eqs. (29) and (30) represent said nonlinear functions for the floating-decoupler and direct-decoupler mounts, respectively. The primary difference between the two functions is the altering

of the x_d^2 term in Eq. (29) to x^2 in Eq. (30) simply because in the direct-decoupler mount the decoupler motion is controlled directly by the input excitation, not by the fluid motion as with the floating-decoupler.

2.2.1. Floating-decoupler mount

To determine the nonlinear equations of motion for the floating-decoupler mount the process is repeated from the linear model with the exception that the momentum equation in Eq. (3). The required change in this equation is the effect of the decoupler closing described by Eq. (29). With this change the nonlinear equations of motion may be written as follows:

$$\begin{bmatrix} M_d & 0 \\ 0 & M_i \end{bmatrix} \begin{Bmatrix} \ddot{x}_d \\ \ddot{x}_i \end{Bmatrix} + \begin{bmatrix} B_d & 0 \\ 0 & B_i \end{bmatrix} \begin{Bmatrix} \dot{x}_d \\ \dot{x}_i \end{Bmatrix} + \begin{bmatrix} A_d^2 K & A_d A_i K \\ A_d A_i K & A_i^2 K \end{bmatrix} \begin{Bmatrix} x_d \\ x_i \end{Bmatrix} + F_{fd} \begin{Bmatrix} 1 \\ 0 \end{Bmatrix} = \frac{A_p}{C_1} \begin{Bmatrix} A_d \\ A_i \end{Bmatrix} x. \tag{31}$$

Because Eq. (31) is nonlinear an exact solution describing the fluid behavior in the frequency domain is impossible; therefore, an approximate closed form solution is sought for Eq. (31) by use of the averaging method. To accomplish such type of solution it becomes necessary to introduce a series of nondimensional parameters by first transforming the time domain the equations are expressed in as a function of the primary linear resonant frequency as follows:

$$\tau = \Omega t, \quad \Omega^2 = \frac{A_d^2 K}{M_d}, \quad x_d = \Delta y_d, \quad x_i = \Delta y_i, \quad x = \Delta y. \tag{32}$$

By using the nondimensional parameters in Eq. (32) the equations of motion in Eq. (31) may be written as follows:

$$\begin{bmatrix} 1 & 0 \\ 0 & 1 \end{bmatrix} \begin{Bmatrix} y_d'' \\ y_i'' \end{Bmatrix} + \begin{bmatrix} \dfrac{B_d + E y_d^2}{M_d \Omega} & 0 \\ 0 & \dfrac{B_i}{M_i \Omega} \end{bmatrix} \begin{Bmatrix} y_d' \\ y_i' \end{Bmatrix} + \begin{bmatrix} 1 & \dfrac{A_i}{A_d} \\ \dfrac{A_i M_d}{A_d M_i} & \dfrac{A_i^2 M_d}{A_d^2 M_i} \end{bmatrix} \begin{Bmatrix} y_d \\ y_i \end{Bmatrix} = \frac{A_p}{C_1 K A_d} \begin{Bmatrix} 1 \\ \dfrac{A_i M_d}{A_d M_i} \end{Bmatrix} y, \tag{33}$$

where

$$y = Y \sin\left(\frac{\omega \tau}{\Omega}\right).$$

To make the equations of motion in Eq. (33) suitable for perturbation analysis the following nondimensional parameters are introduced:

$$w = \frac{\omega}{\Omega}, \quad a = \frac{A_i}{A_d}, \quad m = \frac{M_i}{M_d}, \quad f = \frac{A_p}{C_1 K A_d}, \quad e = \frac{E}{M_d \Omega}, \quad \zeta_d = \frac{B_d}{M_d \Omega}, \quad \zeta_i = \frac{B_i}{M_i \Omega}. \tag{34}$$

Using the nondimensional parameters in Eq. (34) the equations of motion in Eq. (33) may be expressed as follows:

$$\begin{bmatrix} 1 & 0 \\ 0 & 1 \end{bmatrix} \begin{Bmatrix} y_d'' \\ y_i'' \end{Bmatrix} + \begin{bmatrix} \zeta_d + e y_d^2 & 0 \\ 0 & \zeta_i \end{bmatrix} \begin{Bmatrix} y_d' \\ y_i' \end{Bmatrix} + \begin{bmatrix} 1 & a \\ \dfrac{a}{m} & \dfrac{a^2}{m} \end{bmatrix} \begin{Bmatrix} y_d \\ y_i \end{Bmatrix} = fY \begin{Bmatrix} 1 \\ \dfrac{a}{m} \end{Bmatrix} \sin(w\tau). \tag{35}$$

It now becomes convenient to introduce a small parameter as to ensure the forcing amplitude and nonlinearity is small in magnitude

$$\varepsilon = a, \quad \varepsilon d_d = \zeta_d, \quad \varepsilon d_i = \zeta_i, \quad \varepsilon q = e, \quad \varepsilon g = fY, \quad v = \frac{a}{m}. \tag{36}$$

Using the parameters in Eq. (36) the equations of motion in Eq. (35) may be written as follows:

$$y_d'' + \varepsilon\left(d_d + q y_d^2\right) y_d' + y_d + \varepsilon y_i = \varepsilon g \sin(w\tau), \tag{37}$$

$$y_i'' + \varepsilon d_i y_i' + v y_d + \varepsilon v y_i = \varepsilon g v \sin(w\tau). \tag{38}$$

To utilize the averaging method to determine a solution to Eqs. (37) and (38) solutions are assumed as a truncated Taylor series to describe the primary harmonic solution neglecting any sub- or super-harmonic components of the solution while assuming the amplitude and phase terms may be functions of time as

$$y_d = r_d(\tau) \sin\left(w\tau + \phi_d(\tau)\right), \tag{39}$$

$$y_d = r_i(\tau) \sin\left(w\tau + \phi_i(\tau)\right). \tag{40}$$

The derivatives of the solutions expressed in Eqs. (39) and (40) can be expressed as follows:

$$y_d' = r_d(\tau) w \cos\left(w\tau + \phi_d(\tau)\right), \tag{41}$$

$$y_i' = r_i(\tau) w \cos\left(w\tau + \phi_i(\tau)\right), \tag{42}$$

$$y_d'' = r_d'(\tau) w \cos\left(w\tau + \phi_d(\tau)\right) - r_d(\tau) w\left(w + \phi_d'(\tau)\right) \sin\left(w\tau + \phi_d(\tau)\right), \tag{43}$$

$$y_i'' = r_i'(\tau) w \cos\left(w\tau + \phi_i(\tau)\right) - r_i(\tau) w\left(w + \phi_i'(\tau)\right) \sin\left(w\tau + \phi_i(\tau)\right), \tag{44}$$

where

$$r_d'(\tau) \sin\left(w\tau + \phi_d(\tau)\right) + r_d(\tau)\phi_d'(\tau) \cos\left(w\tau + \phi_d(\tau)\right) = 0, \tag{45}$$

$$r_i'(\tau) \sin\left(w\tau + \phi_i(\tau)\right) + r_i(\tau)\phi_i'(\tau) \cos\left(w\tau + \phi_i(\tau)\right) = 0. \tag{46}$$

At this point it becomes advantageous to introduce the following parameters

$$\psi_d = w\tau + \phi_d, \tag{47}$$

$$\psi_i = w\tau + \phi_i. \tag{48}$$

Substitution of Eqs. (39)–(44) into the equations of motion given in Eqs. (37) and (38) and utilizing the parameters in Eqs. (47) and (48) allows the governing second-order equations given in Eqs. (37) and (38) to be written as a system of first-order differential equations that vary slowly over one period of oscillation (2π) [11] as follows:

$$r'_d = -\tfrac{1}{2}\varepsilon d_d r_d - \tfrac{1}{2}\varepsilon g\cos\left(\phi_d\right), \tag{49}$$

$$r_d\phi'_d = \tfrac{1}{2}\varepsilon v r_d - r_d(w-1) - \tfrac{1}{2}\varepsilon g\sin\left(\phi_d\right) + \tfrac{1}{8}\varepsilon q r_d^3, \tag{50}$$

$$r'_i = -\tfrac{1}{2}\varepsilon d_i r_i + \tfrac{1}{2}\varepsilon g v\cos\left(\phi_i\right), \tag{51}$$

$$r'_i = -\tfrac{1}{2}\varepsilon d_i r_i + \tfrac{1}{2}\varepsilon g v\cos\left(\phi_i\right). \tag{52}$$

For the solution to the governing equations in Eqs. (37) and (38) to be steady-state in nature the solutions of Eqs. (49)–(52) cannot vary with time; therefore, the time derivatives in said equations must vanish. Solving the resulting equations for the trigonometric terms and using the identity $\sin^2 + \cos^2 = 1$ yields the following implicit frequency response functions describing the nondimensional amplitude of the decoupler and inertia track. Using the said trigonometric terms also allows description of the phase angle equations for both the decoupler and the inertia track as follows:

$$\left(\frac{r_d\left(8(1-w)+4\varepsilon v+\varepsilon q r_d^2\right)}{4\varepsilon g}\right)^2 + \left(\frac{d_d r_d}{g}\right)^2 = 1, \tag{53}$$

$$\left(\frac{r_i(2(1-w)+\varepsilon v)}{\varepsilon g v}\right)^2 + \left(\frac{d_i r_i}{g v}\right)^2 = 1, \tag{54}$$

$$\phi_d = \arctan\left(\frac{8(1-w)+4\varepsilon v+\varepsilon q r_d^2}{4\varepsilon d_d}\right), \tag{55}$$

$$\phi_i = -\arctan\left(\frac{2(w-1)-\varepsilon v}{\varepsilon d_i}\right). \tag{56}$$

Because the steady-state motion of the solution is nonlinear no explicit frequency domain solution may be determined. More specifically, because of the possibility for existence of jump phenomenon-type behavior in nonlinear systems the amplitude of oscillation may not be directly

expressed as a function of frequency noting that if a jump occurs such a function would be required to supply two stable solutions and one unstable solution at a specific range of frequency values. Such behavior cannot be described by a function noting the requirement for a function to be single-valued; therefore, the frequency response functions must be specified implicitly as in Eqs. (53) and (54) [11].

To proceed with the frequency response analysis the transmitted force equation may be written similar to the approach for the linear model. The format has been switched to dimensional variables for ease of description as follows:

$$f_T = K_r X \sin(\omega t) + B_r X \omega \cos(\omega t) + A_p p_1 \sin\left(\omega t + \phi_1\right). \tag{57}$$

Note that the solution being sought after may be expressed by $f_T = F_T \sin(\omega t + \phi_{\text{sys}})$; therefore, after use of the appropriate identities Eq. (57) may be expressed in the frequency domain as follows:

$$F_T = \sqrt{X\left(K_r G_1 + B_r \omega G_2 + A_p^2 p_1^2\right)}, \tag{58}$$

$$\phi_{\text{sys}} = \arctan\left(\frac{B_r X \omega + A_p p_1 \sin\left(\phi_1\right)}{K_r X + A_p p_1 \cos\left(\phi_1\right)}\right), \tag{59}$$

where

$$G_1 = K_r X + 2A_p p_1 \cos\left(\phi_1\right),$$

$$G_2 = B_r X \omega + 2A_p p_1 \sin\left(\phi_1\right).$$

The pressure term in Eqs. (58) and (59) may be defined by using the continuity equation given in Eq. (5) and the frequency response functions given in Eqs. (53)–(56).

$$p_1 \omega \cos\left(\omega t + \phi_1\right) = \frac{\omega}{C_1}\left(A_p X \cos(\omega t) - \left(A_d R_d \cos\left(\omega t + \phi_d\right) + A_i R_i \cos\left(\omega t + \phi_i\right)\right)\right), \tag{60}$$

where

$$R_d = \Delta r_d, \quad R_i = \Delta r_i.$$

Using the appropriate trigonometric identities in conjunction with Eq. (60) p_1 and ϕ_1 may be expressed as follows:

$$p_1 = \frac{1}{C_1}\sqrt{A_p X H_1 + A_d R_d H_2 + H_3}, \tag{61}$$

$$\phi_1 = \arctan\left(\frac{A_d R_d \sin\left(\phi_d\right) + A_i R_i \sin\left(\phi_i\right)}{A_p X - \left(A_d R_d \cos\left(\phi_d\right) + A_i R_i \cos\left(\phi_i\right)\right)}\right), \tag{62}$$

where

$$H_1 = A_p X - 2A_i R_i \cos(\phi_i),$$

$$H_2 = A_d R_d - 2A_p X \cos(\phi_d),$$

$$H_3 = A_i^2 R_i^2 + 2A_d A_i R_d R_i \cos(\phi_d - \phi_i).$$

Using Eq. (58) the dynamic stiffness equation may be written as follows:

$$K_{\text{dyn}} = \frac{F_T}{X} = \frac{1}{X}\sqrt{X\left(K_r G_1 + B_r \omega G_2 + A_p^2 p_1^2\right)}. \tag{63}$$

2.2.2. Direct-decoupler mount

The nonlinear model for the direct-decoupler mount can be determined from the linear model, in the same manner as the nonlinear model for the floating-decoupler mount, simply by adding the nonlinear decoupler function expressed in Eq. (30) as follows:

$$\begin{bmatrix} M_d & 0 \\ 0 & M_i \end{bmatrix}\begin{Bmatrix} \ddot{x}_d \\ \ddot{x}_i \end{Bmatrix} + \begin{bmatrix} B_d & 0 \\ 0 & B_i \end{bmatrix}\begin{Bmatrix} \dot{x}_d \\ \dot{x}_i \end{Bmatrix} + \begin{bmatrix} A_d^2 K & -\dfrac{A_d A_i}{C_2} \\ -\dfrac{A_d A_i}{C_2} & \dfrac{A_i^2}{C_2} \end{bmatrix}\begin{Bmatrix} x_d \\ x_i \end{Bmatrix} + F_{\text{dd}}\begin{Bmatrix} 1 \\ 0 \end{Bmatrix}$$
$$= \begin{Bmatrix} A_d\left(\dfrac{A_p}{C_1} - A_B K\right) \\ \dfrac{A_i A_B}{C_2} \end{Bmatrix} x. \tag{64}$$

Notice, however, that the nonlinearity introduced by the addition of F_{dd} transforms the equations of motion into a parametric system of equations. Because the system is parametric there is no guarantee that for all possible mount configurations there exists a periodic solution. To ensure a periodic response exists the stability of the system must be analyzed. To accomplish a stability analysis for a system of parametric differential equations the governing equations should be transformed into a nondimensional form, similar to the process outlined for the floating-decoupler mount. After transformation of the equations of motion into a nondimensional form the energy-rate method should be employed [12]. The output of the energy-rate method is the stability diagram for the system.

To achieve a nondimensional system of equations a nondimensional time format will be introduced along with nondimensional position variables in a similar manner to that used for the floating-decoupler mount

$$\tau = \Omega t, \quad \Omega^2 = \frac{A_d^2 K}{M_d}, \quad x_d = \Delta y_d, \quad x_i = \Delta y_i, \quad x = \Delta y. \tag{65}$$

Using the parameters in Eq. (65) the equations of motion given in Eq. (64) may be written as follows:

$$\begin{bmatrix} 1 & 0 \\ 0 & 1 \end{bmatrix} \begin{Bmatrix} y_d'' \\ y_i'' \end{Bmatrix} + \begin{bmatrix} \dfrac{B_d + Ey^2}{M_d\Omega} & 0 \\ 0 & \dfrac{B_i}{M_i\Omega} \end{bmatrix} \begin{Bmatrix} y_d' \\ y_i' \end{Bmatrix} + \begin{bmatrix} 1 & -\dfrac{A_i}{A_d C_2 K} \\ -\dfrac{A_i M_d}{A_d M_i C_2 K} & \dfrac{A_i^2 M_d}{A_d^2 M_i C_2 K} \end{bmatrix} \begin{Bmatrix} y_d \\ y_i \end{Bmatrix} = \begin{Bmatrix} \dfrac{A_p}{A_d C_1 K} - \dfrac{A_B}{A_d} \\ \dfrac{A_i A_B M_d}{A_d^2 M_i C_2 K} \end{Bmatrix} y, \tag{66}$$

where

$$y = Y \sin\left(\frac{\omega\tau}{\Omega}\right).$$

To further simplify the governing equations in Eq. (66) the following nondimensional parameters are introduced:

$$w = \frac{\omega}{\Omega}, \quad a = \frac{A_i}{A_d}, \quad m = \frac{M_i}{M_d}, \quad f = \frac{A_p}{C_1 K A_d}, \quad e = \frac{E}{M_d\Omega}, \quad \zeta_d = \frac{B_d}{M_d\Omega},$$
$$\zeta_i = \frac{B_i}{M_i\Omega}, \quad \alpha = \frac{A_B}{A_d}, \quad u = \frac{1}{C_2 K}. \tag{67}$$

Using the parameters in Eq. (67) the governing equations in Eq. (66) may be written as follows:

$$\begin{bmatrix} 1 & 0 \\ 0 & 1 \end{bmatrix} \begin{Bmatrix} y_d'' \\ y_i'' \end{Bmatrix} + \begin{bmatrix} \zeta_d + eY^2 \sin^2(w\tau) & 0 \\ 0 & \zeta_i \end{bmatrix} \begin{Bmatrix} y_d' \\ y_i' \end{Bmatrix} + \begin{bmatrix} 1 & -au \\ -\dfrac{au}{m} & \dfrac{a^2 u}{m} \end{bmatrix} \begin{Bmatrix} y_d \\ y_i \end{Bmatrix} = \begin{Bmatrix} f - \alpha \\ \dfrac{a\alpha u}{m} \end{Bmatrix} Y \sin(w\tau). \tag{68}$$

To make Eq. (68) suitable for use by the energy-rate method the following terms are introduced:

$$\varepsilon = a, \quad \varepsilon d_d = \zeta_d, \quad \varepsilon d_i = \zeta_i, \quad v = \frac{a}{m}, \quad \varepsilon g = fY,$$
$$\varepsilon h = \alpha Y, \quad \varepsilon\gamma = eY^2. \tag{69}$$

Using the parameters in Eq. (69) the final form of the governing equations may be written as follows:

$$y_d'' + \varepsilon\big(d_d + \gamma \sin^2(w\tau)\big) y_d' + y_d - \varepsilon u y_i = \varepsilon(g - h)\sin(w\tau), \tag{70}$$

$$y_i'' + \varepsilon d_i y_i' - vu y_d + \varepsilon vu y_i = \varepsilon vhu \sin(w\tau). \tag{71}$$

To analyze the stability of the system governed by Eqs. (70) and (71) it becomes advantageous to introduce a small term to perturb the steady-state solution as

$$y_d = y_{d0} + z_d, \tag{72}$$

$$y_i = y_{i0} + z_i. \tag{73}$$

Eqs. (72) and (73) illustrate the steady-state solution (y_{d0} and y_{i0}) perturbed by small parameters z_d and z_i. Substitution of these equations into Eqs. (70) and (71) yields the following:

$$y''_{d0} + z''_d + \varepsilon\big(d_d + \gamma \sin^2(w\tau)\big)\big(y'_{d0} + z'_d\big) + y_{d0} + z_d - \varepsilon u\big(y_{i0} + z_i\big) = \varepsilon(g-h)\sin(w\tau), \tag{74}$$

$$y''_{i0} + z''_i + \varepsilon d_i\big(y'_{i0} + z'_i\big) - vu\big(y_{d0} + z_d\big) + \varepsilon vu\big(y_{i0} + z_i\big) = \varepsilon vhu \sin(w\tau). \tag{75}$$

Noting that y_{d0} and y_{i0} represent steady-state solutions to Eqs. (70) and (71), Eqs. (74) and (75) may be simplified and written as follows:

$$z''_d + \varepsilon\big(d_d + \gamma \sin^2(w\tau)\big)z'_d + z_d - \varepsilon u z_i = 0, \tag{76}$$

$$z''_i + \varepsilon d_i z'_i - vuz_d + \varepsilon vuz_i = 0. \tag{77}$$

The energy-rate method may be applied to Eqs. (76) and (77) by defining the rate of change of the total energy of the system [12]. Because this system contains two dof the energy-rate equations must be determined for each respective dof

$$U'_d = -z'_d\big(\varepsilon\big(d_d + \gamma \sin^2(w\tau)\big)z'_d - \varepsilon u z_i\big), \tag{78}$$

$$U'_i = -z'_i\big(\varepsilon d_i z'_i - vuz_d\big). \tag{79}$$

To determine whether or not a periodic solution exists for a specific combination of w and γ the energy-rate equations given in Eqs. (78) and (79) are integrated over one period [12].

$$U_{d,\,\mathrm{avg}} = \frac{1}{T}\int_0^T U'_d \,\mathrm{d}\tau, \tag{80}$$

$$U_{i,\,\mathrm{avg}} = \frac{1}{T}\int_0^T U'_i \,\mathrm{d}\tau, \tag{81}$$

where

$$T = \frac{2\pi}{\eta\omega_1 + \chi\omega_2}, \quad \omega_1 = 1, \quad \omega_2 = \sqrt{\varepsilon vhu}, \quad \eta, \chi \in \Psi.$$

The results of the integration in Eqs. (80) and (81) are illustrated in Figs. 7 and 8.

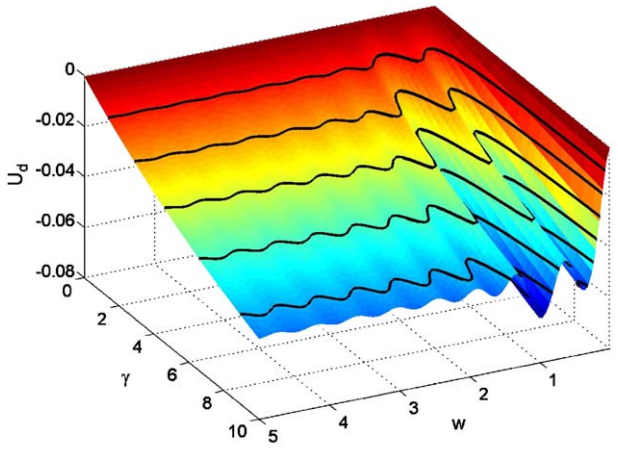

Fig. 7. Energy integral surface relating to the decoupler dof.

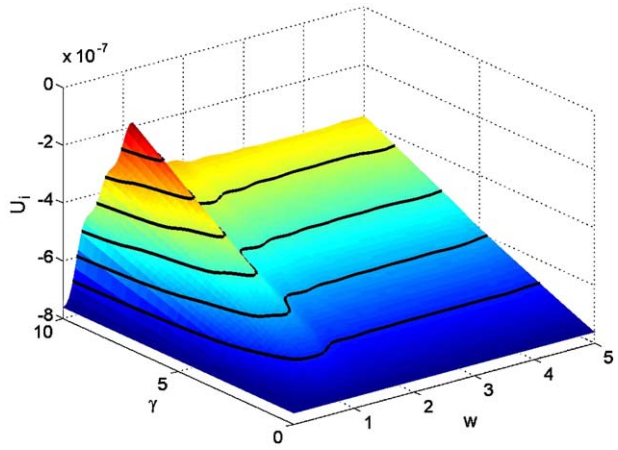

Fig. 8. Energy integral surface relating to the inertia track dof.

Figs. 7 and 8 illustrate the energy integral surface that is a direct result of the energy-rate method. Wherever said integral is less than zero the system exhibits stable behavior. Wherever the energy integral surface equals zero exactly the system exhibits perfectly periodic behavior, and if the energy integral surface is positive the system exhibits unstable behavior. Because both surfaces illustrated in Figs. 7 and 8 lie completely below the zero plane they are everywhere stable for the combination of parameters investigated. Notice, however, that only two parameters are investigated while the equations of motion contained several more parameters. The parameters w and γ were utilized as they directly relate to the parametric system behavior whereas any other parameters do not (see Table 1 for property values).

Knowing the direct-decoupler mount is stable suggests that a periodic-type response is possible, and assuming that such a solution can be obtained a frequency response should be obtainable for this mount. With that said the averaging method is applied to the governing equations by

Table 1
Values for hydraulic mount

Symbol	Floating-decoupler	Direct-decoupler	Unit
A_i	5.72E−5	5.72E−5	m^2
A_d	2.30E−3	2.30E−3	m^2
A_p	5.027E−3	5.027E−3	m^2
A_B	—	3.393E−3	m^2
B_i	2.90	2.90	N s/m
B_d	4.83E−3	4.83E−3	N s/m
B_r	2000	2000	N s/m
C_1	4.60E−10	4.60E−10	m^5/N
C_2	4.60E−8	4.60E−9	m^5/N
C_3	—	4.60E−8	m^5/N
K	2.196E9	2.413E9	N/m^5
K_r	266E3	266E3	N/m
M_i	0.37E−2	0.37E−2	kg
M_d	2.645E−2	2.645E−2	kg
E	2.9095	2.9095	—
Δ	1.0E−3	1.0E−3	m
X	1.0E−3	1.0E−3	m
η	—	1	—
χ	—	1	—

introducing the following assumed solutions to the steady-state motion:

$$y_d = a_d(\tau)\sin(w\tau) + b_d(\tau)\cos(w\tau), \tag{82}$$

$$y_i = a_i(\tau)\sin(w\tau) + b_i(\tau)\cos(w\tau). \tag{83}$$

Using Eqs. (82) and (83) the time derivatives of the system may be expressed as follows:

$$y'_d = w(a_d(\tau)\cos(w\tau) - b_d(\tau)\sin(w\tau)), \tag{84}$$

$$y'_i = w(a_i(\tau)\cos(w\tau) - b_i(\tau)\sin(w\tau)), \tag{85}$$

$$y''_d = w\big(a'_d(\tau)\cos(w\tau) - b'_d(\tau)\sin(w\tau) - w(a_d(\tau)\sin(w\tau) + b_d(\tau)\cos(w\tau))\big), \tag{86}$$

$$y''_i = w\big(a'_i(\tau)\cos(w\tau) - b'_i(\tau)\sin(w\tau) - w(a_i(\tau)\sin(w\tau) + b_i(\tau)\cos(w\tau))\big), \tag{87}$$

where

$$a'_d(\tau)\sin(w\tau) + b'_d(\tau)\cos(w\tau) = 0, \tag{88}$$

$$a'_i(\tau)\sin(w\tau) + b'_i(\tau)\cos(w\tau) = 0. \tag{89}$$

The assumed solutions in Eqs. (82) and (83) in conjunction with the time derivatives defined in Eqs. (84)–(87) are now substituted into Eqs. (70) and (71). By using the resulting expressions in conjunction with Eqs. (88) and (89) a system of first-order differential equations may be obtained.

Assuming the solution is slowly varying over one period of oscillation the system of equations may be written as follows:

$$a'_d = \frac{1}{8w}\left(4b_d\left(w^2-1\right)+4\varepsilon u b_i - \varepsilon a_d w(4d_d+\gamma)\right), \tag{90}$$

$$b'_d = \frac{1}{8w}\left(4\varepsilon h + 4a_d\left(1-w^2\right) - \varepsilon b_d w(4d_d+3\gamma) - 4\varepsilon u a_i - 4\varepsilon g\right), \tag{91}$$

$$a'_i = \frac{1}{2w}\left(b_i\left(w^2-\varepsilon v u\right) - \varepsilon d_i a_i w + v u b_d\right), \tag{92}$$

$$b'_i = \frac{1}{2w}\left(a_i\left(\varepsilon v u - w^2\right) - v u a_d - \varepsilon d_i b_i w - \varepsilon h v u\right). \tag{93}$$

Noting that for a steady-state solution the time derivatives in Eqs. (90)–(93) must be zero; therefore, after solving for the amplitude terms (a_d, b_d, a_i, b_i) the frequency response functions for the system may be written as follows:

$$r_d = \sqrt{a_d^2 + b_d^2}, \tag{94}$$

$$r_i = \sqrt{a_i^2 + b_i^2}, \tag{95}$$

$$\phi_d = \arctan\left(\frac{b_d}{a_d}\right), \tag{96}$$

$$\phi_i = \arctan\left(\frac{b_i}{a_i}\right). \tag{97}$$

Eqs. (94) and (95) are the frequency response functions for the amplitude of the fluid column motion and Eqs. (96) and (97) define the phase lag for the decoupler and inertia track.

$$\begin{aligned} f_T = {} & K_r X \sin(\omega t) + B_r X \omega \cos(\omega t) + A_p p_1 \sin\left(\omega t + \phi_1\right) \\ & + A_B \omega\left(p_2 \sin\left(\omega t + \phi_2\right) - p_1 \sin\left(\omega t + \phi_1\right)\right). \end{aligned} \tag{98}$$

As before a solution is sought as $f_T = F_T \sin(\omega t + \phi_{\text{sys}})$; therefore, after using the appropriate identities the transmitted force may be described in the frequency domain as follows:

$$F_T = \sqrt{(B_r X\omega)^2 - 2B_r X\omega S_1 + (K_r X)^2 - 2K_r X S_2 - A_B^2 S_3 + 2A_B A_p p_1 S_4 + \left(A_p p_1\right)^2}, \tag{99}$$

$$\phi_{\text{sys}} = \arctan\left(\frac{B_r X\omega - S_1}{K_r X - S_2}\right), \tag{100}$$

where

$$S_1 = A_B\left(p_1 \sin\left(\phi_1\right) - p_2 \sin\left(\phi_2\right)\right) - A_p p_1 \sin\left(\phi_1\right),$$

$$S_2 = A_B\left(p_1 \cos\left(\phi_1\right) - p_2 \cos\left(\phi_2\right)\right) - A_p p_1 \cos\left(\phi_1\right),$$

$$S_3 = 2p_1p_2\cos(\phi_2 - \phi_1) - p_1^2 - p_2^2,$$

$$S_4 = p_2\cos(\phi_2 - \phi_1) - p_1.$$

The pressure terms in Eqs. (99) and (100) may be expressed as follows:

$$p_1 = \frac{\sqrt{A_dR_dJ_1 + X^2J_2}}{C_1}, \tag{101}$$

$$p_2 = \frac{\sqrt{(A_BX)^2J_3 + 2A_BX(C_2+C_3)J_4 + (A_dR_d)^2J_3 - 2A_dA_iR_dR_iJ_5 + (A_iR_iC_3)^2}}{C_2C_3}, \tag{102}$$

$$\phi_1 = -\arctan\left(\frac{A_dR_d\cos(\phi_d) + X(A_B - A_p)}{A_dR_d\sin(\phi_d)}\right), \tag{103}$$

$$\phi_2 = -\arctan\left(\frac{(C_2+C_3)(A_BX + A_dR_d\cos(\phi_d)) - A_iR_iC_3\cos(\phi_i)}{(C_2+C_3)A_dR_d\sin(\phi_d) - A_iR_iC_3\sin(\phi_i)}\right), \tag{104}$$

where

$$J_1 = A_dR_d + 2X\cos(\phi_d)(A_B - A_p),$$

$$J_2 = A_B^2 + A_p^2 - 2A_BA_p,$$

$$J_3 = C_2^2 + 2C_2C_3 + C_3^2,$$

$$J_4 = A_dR_d\cos(\phi_d)(C_2+C_3) - A_iR_iC_3\cos(\phi_i),$$

$$J_5 = C_3(C_2 - C_3)\cos(\phi_d - \phi_i),$$

$$R_d = \Delta r_d, \quad R_i = \Delta r_i.$$

Using Eqs. (99)–(104) the dynamic stiffness equation may be written as follows:

$$K_{\text{dyn}} = \frac{F_T}{X} = \frac{1}{X}\sqrt{(B_rX\omega)^2 - 2B_rX\omega S_1 + (K_rX)^2 - 2K_rXS_2 - A_B^2S_3 + 2A_BA_pp_1S_4 + (A_pp_1)^2}. \tag{105}$$

3. Results

To obtain a good comparison between each mount the parameters describing each mount are kept constant. Table 1 illustrates the values used for describing each engine mount.

Table 2 illustrates the natural frequencies of the linear models for both engine mounts. From this table it may be seen that by placing the inertia track in parallel with decoupler decreases the natural frequencies (floating-decoupler mount) with respect to the direct-decoupler mount in which the inertia track is in series with the decoupler. In addition, by placing the inertia track in

parallel with an open decoupler, as in the linear model, the lower natural frequency is practically zero indicating an almost disconnected state for the degree of freedom corresponding to said natural frequency. This indicates that the primary means for flow between chambers is through the decoupler, and the inertia track plays little role in the flow between chambers. Intuitively this makes sense because the decoupler has a much larger cross-sectional area and damping coefficient when compared with the inertia track, and therefore should provide the greater flow. However, it may be seen from Table 2 that by placing the decoupler and inertia track in series (direct-decoupler mount) forces use of the inertia track; therefore, the resonant frequency corresponding to the inertia track becomes further from zero indicating an increase in the use of the inertia track.

Figs. 9 and 10 illustrate a comparison between the linear models describing both mounts. Fig. 9 illustrates the force transmitted by each mount across the frequency spectrum whereas Fig. 10 illustrates the system phase lag. Both figures tend to indicate that the direct decoupler mount is more heavily damped throughout the frequency spectrum, most notably low frequencies, but this is most easily attributed to the lack of decoupler closing action associated with the floating-decoupler mount.

Fig. 11 illustrates the decoupler flow rate frequency response for the floating-decoupler mount. The jump phenomenon commonly associated with nonlinear systems is readily apparent in Fig. 11 around the primary resonant frequency [11].

Fig. 12 illustrates the transmitted force predicted by both the linear and nonlinear models for the floating-decoupler type mount. Here, the nonlinearity of the system induces a "frequency

Table 2
Linear model natural frequency comparison

	f_1 (Hz)	f_2 (Hz)
Floating-decoupler	105.70	7.59E−8
Direct-decoupler	110.57	2.10

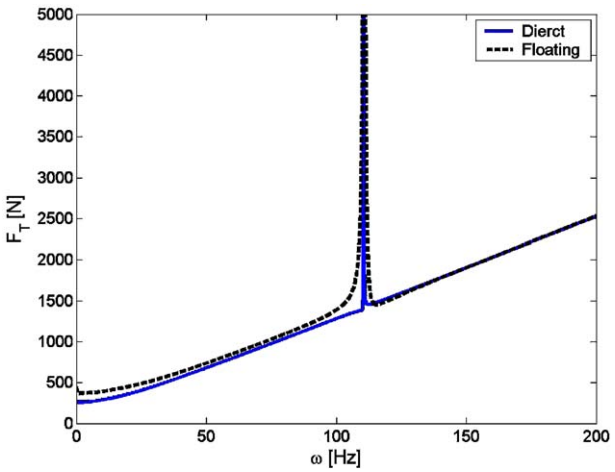

Fig. 9. Linear model transmitted force comparison.

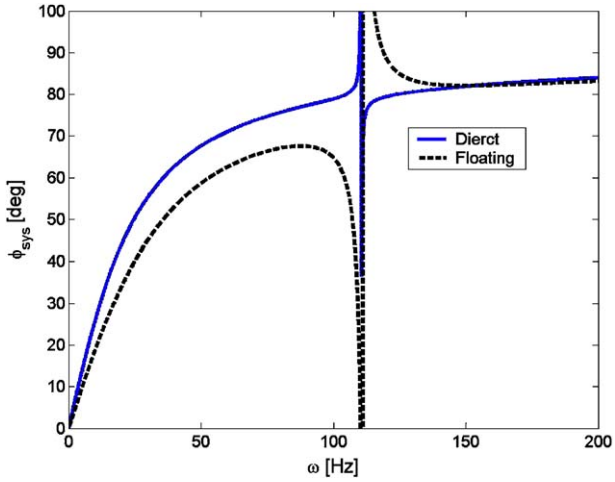

Fig. 10. Linear model phase lag comparison.

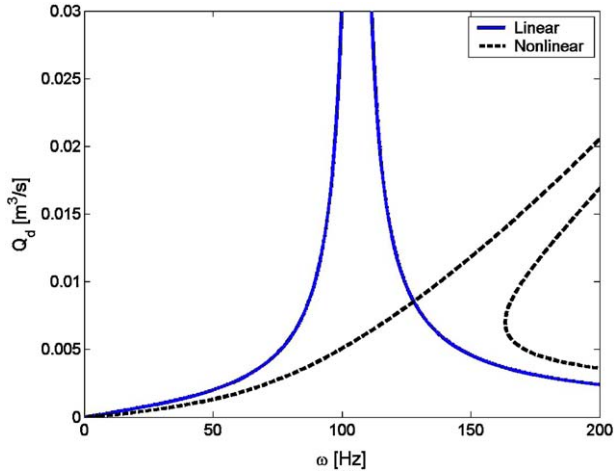

Fig. 11. Decoupler flow rate (floating-decoupler mount).

island'' of sorts beyond the maximum resonant frequency. This ''island'' is illustrated by some nonlinear systems indicating further existence of unstable solutions. At frequency points where the island exists the steady-state solution may exist at three separate points where two are stable solutions and one is unstable, similar to the situation of jump phenomenon.

Fig. 12 also illustrates good agreement below primary resonance between the linear and nonlinear models. The discrepancy between solutions increases slightly after primary resonance because of the jump condition associated with the decoupler motion; hence, the appearance of the frequency island.

Fig. 13 illustrates the dynamic stiffness of the floating-decoupler mount as predicted by both the linear and nonlinear models. Fig. 14 illustrates the phase lag predicted by both the linear and nonlinear models.

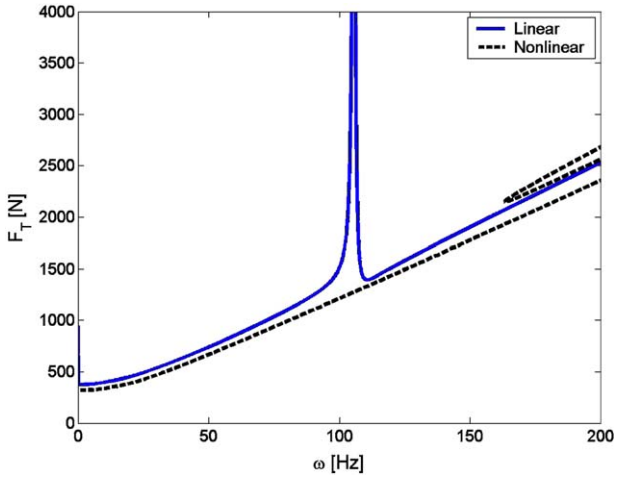

Fig. 12. Transmitted force (floating-decoupler mount).

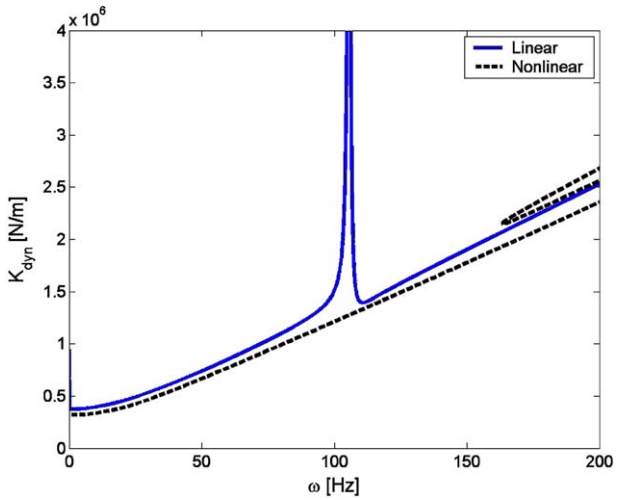

Fig. 13. Dynamic stiffness (floating-decoupler mount).

Fig. 15 illustrates the decoupler flow rate frequency response for both the linear and nonlinear models describing the direct-decoupler mount. Here, the additional damping provided by the addition of the nonlinear function is readily noted by the decreased amplitude near resonance for the nonlinear model as compared to the linear model.

Fig. 16 illustrates the force transmitted to the base of the direct-decoupler mount as predicted by both the linear and nonlinear models. Again the linear and nonlinear models agree almost exactly with the exception of the frequency region surrounding primary resonance (see Table 2). In this region the additional flow resistance through the closing decoupler provides additional damping not accounted for in the linear model thereby decreasing the peak amplitude near resonance (see Fig. 15). In addition, the agreement of the linear and nonlinear models throughout the frequency domain indicates that the averaging method provided an acceptable solution noting

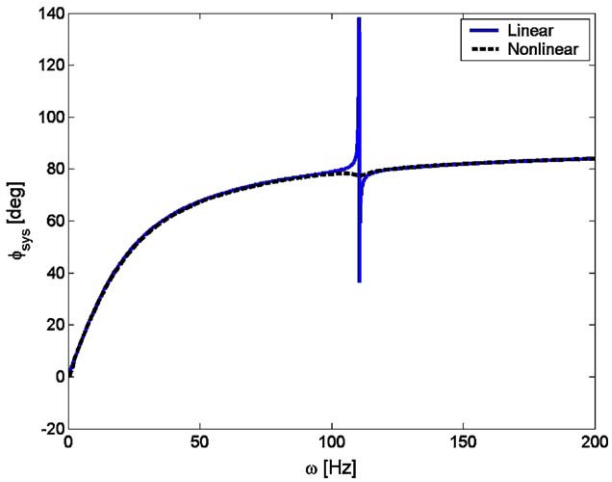

Fig. 14. Phase lag (floating-decoupler mount).

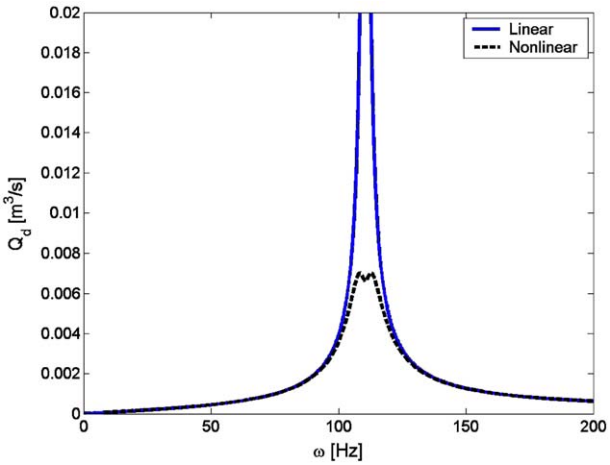

Fig. 15. Decoupler flow rate (direct-decoupler mount).

the linear solution is mathematically exact. However, one point of interest is the accuracy with which the linear model predicts system behavior throughout the frequency domain.

Fig. 17 illustrates the dynamic stiffness of the direct-decoupler mount again illustrating the results predicted by both the linear and nonlinear models. Fig. 18 illustrates the overall system phase lag for the linear and nonlinear models.

Because the nonlinear models consider the effects of the decoupler closing action they most appropriately model the actual mount behavior; therefore, it is only appropriate that the nonlinear models for each mount be compared directly as to ascertain information regarding the benefits of either design.

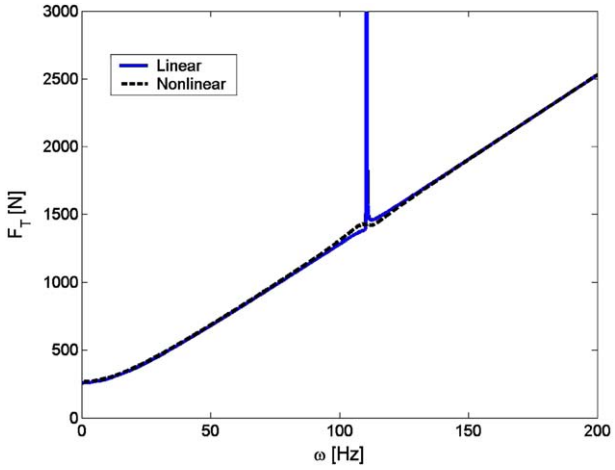

Fig. 16. Transmitted force (direct-decoupler mount).

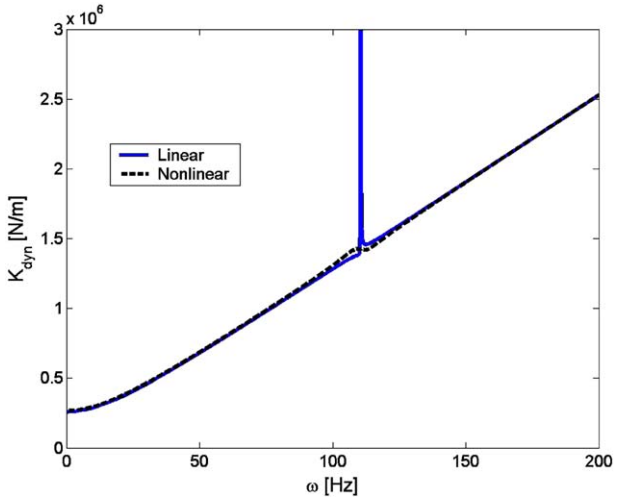

Fig. 17. Dynamic stiffness (direct-decoupler mount).

Fig. 19 illustrates the flow rate through the decoupler of each mount as predicted by the nonlinear models. Fig. 20 illustrates the force transmitted by each mount, Fig. 21 illustrates the dynamic stiffness of each mount, and Fig. 22 illustrates the phase lag for each mount. As illustrated by Fig. 20 both mounts transmit an approximately equivalent force amplitude to the chassis of the vehicle throughout the frequency spectrum with the exception of each mounts respective resonant domains. The direct-decoupler mount exhibits a slight spike in transmissibility at its primary resonant frequency of ~110 Hz. Whereas the floating-decoupler mount does not exhibit such a spike in transmissibility. Instead this mount exhibits a frequency island-type phenomenon at frequencies above 150 Hz. Even though both mounts are approximately equivalent in isolation capabilities across the frequency spectrum the direct-decoupler mount

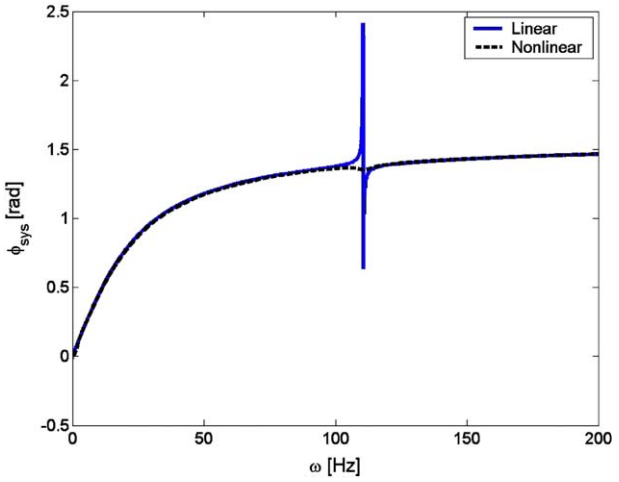

Fig. 18. Phase lag (direct-decoupler mount).

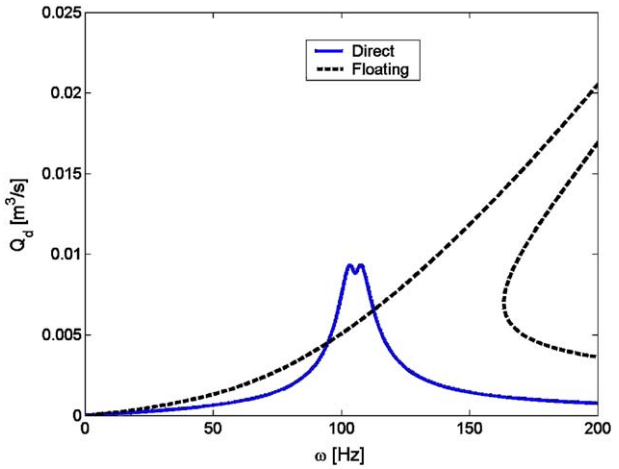

Fig. 19. Decoupler flow rate (nonlinear model comparison).

exhibits slightly better isolation characteristics below 25 Hz whereas the floating-decoupler-type mount exhibits slightly better behavior in frequencies above resonance. This is most likely due to the manner in which the inertia track and decoupler are laid out. Recall that in the direct-decoupler design the inertia track and decoupler are in series thereby forcing the inertia track into service regardless of the frequency or amplitude of excitation; however, the amount of inertia track activity depends strongly on the amplitude of excitation. In contrast, the floating-decoupler design places the decoupler and inertia track in parallel thereby allowing the chamber pressure differences to dictate the behavior of each component. Notice that during low-frequency excitations the decoupler is typically forced into a closed position thereby leaving the inertia track as the only means for appreciable equalization of pressure. However, in the direct-decoupler

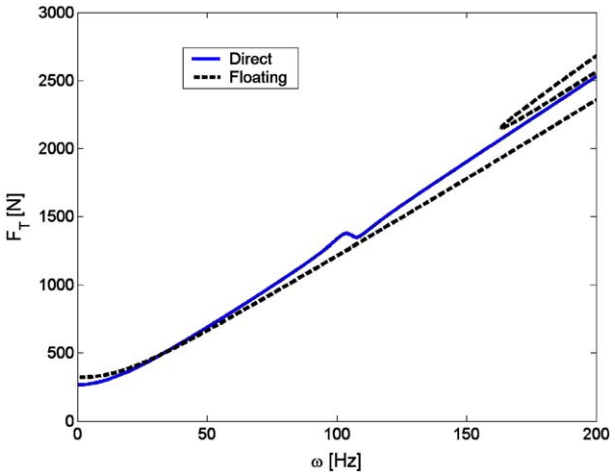

Fig. 20. Transmitted force (nonlinear model comparison).

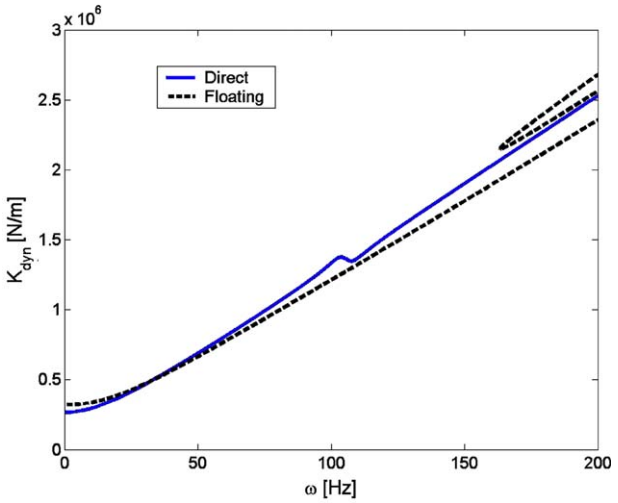

Fig. 21. Dynamic stiffness (nonlinear model comparison).

mount the motion of the decoupler actually forces fluid into the inertia track thereby providing additional damping from not only the inertia track activity but the motion of the decoupler as well. In the low-frequency region (below ~25 Hz) the additional damping provided by the direct-decoupler mount improves the transmissibility of the mount. However, the same may not be said for higher frequencies above resonance in which a lower overall damping coefficient is desired for reduced transmissibility. In this region the floating-decoupler mount is superior simply because the decoupler does not typically bottom out and therefore chamber pressure differences are equalized via the decoupler and the inertia track is basically short-circuited. Fig. 22 illustrates the

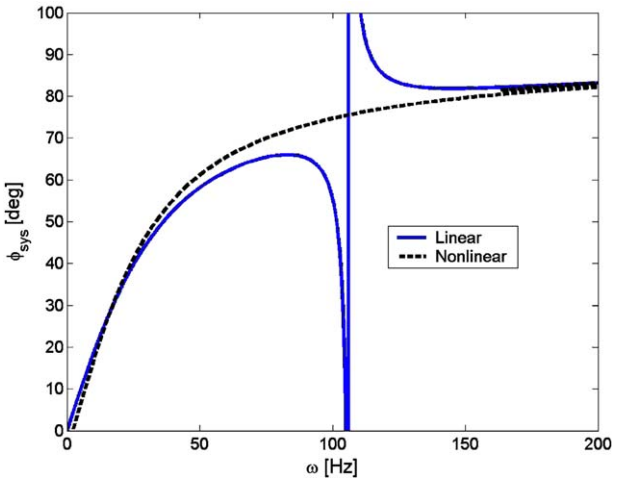

Fig. 22. Phase lag (nonlinear model comparison).

above concept quite well in showing the differences in phase lag between the two mounts in the aforementioned frequency regions.

4. Conclusions

This paper has investigated the frequency domain behavior of two different designs of passive hydraulic engine mounts by use of appropriate linear and nonlinear models. A design relying on fluid pressure changes induced by engine/road excitations to control the amplitude-sensitive component of the mount was compared with a design that controlled the mount behavior by directly using the engine/road excitations. When both mount are designed in a similar manner such that the properties of each mount are constant with respect to one another the isolation characteristics of either mount are similar; however, each respective mount has its advantages and disadvantages as compared to one another. The direct-decoupler mount exhibits the lowest transmissibility in low-frequency domains whereas the floating-decoupler mount behaves better as excitation frequencies increase. In addition to comparing the performance of the two engine mounts several mathematical difficulties were investigated. The instabilities of the direct-decoupler-type mount were investigated using a rather new technique described as the energy-rate method introduced as an effective method to analyze the stability of the parametric system. In addition, the nonlinear frequency response solutions for both mounts are validated by direct comparison to their corresponding linear counterparts and noting the similarity between solutions in regions sufficiently removed from resonance the nonlinear modeling is considered accurate. The appearance of jump phenomenon related instabilities in the frequency response of the floating-decoupler mount is shown to exist, which is consistent with published literature on the subject of nonlinear modeling of hydraulic mounts. In addition, the existence of a frequency island has been illustrated in the high-frequency region of operation for the floating-decoupler-type hydraulic mount.

Appendix A

A.1. Linear model laplace transformations

A.1.1. Floating-decoupler mount (linear model)

$$\begin{Bmatrix} X_d(s) \\ X_i(s) \end{Bmatrix} = \frac{A_p}{C_1|\mathbf{D}|} \begin{Bmatrix} A_d\left(s^2M_i + sB_i + A_i^2K\right) - A_i(A_dA_iK) \\ -A_d(A_dA_iK) + A_i\left(s^2M_d + sB_d + A_d^2K\right) \end{Bmatrix}, \tag{A.1}$$

where

$$\mathbf{D} = \begin{bmatrix} s^2M_d + sB_d + A_d^2K & A_dA_iK \\ A_dA_iK & s^2M_i + sB_i + A_i^2K \end{bmatrix}.$$

A.1.2. Direct-decoupler mount (linear model)

$$\begin{Bmatrix} X_d(s) \\ X_i(s) \end{Bmatrix} = \frac{1}{|\mathbf{D}|} \begin{Bmatrix} A_d\left(\frac{A_p}{C_1} - A_BK\right)\left(s^2M_d + sB_d + A_d^2K\right) + \frac{A_i^2A_dA_B}{C_2^2} \\ \frac{A_d^2A_i}{C_2}\left(\frac{A_p}{C_1} - A_BK\right) + \frac{A_iA_B}{C_2}\left(s^2M_d + sB_d + A_d^2K\right) \end{Bmatrix}, \tag{A.2}$$

where

$$\mathbf{D} = \begin{bmatrix} s^2M_d + sB_d + A_d^2K & -\frac{A_dA_i}{C_2} \\ -\frac{A_dA_i}{C_2} & s^2M_i + sB_i + \frac{A_i^2}{C_2} \end{bmatrix}.$$

References

[1] W.C. Flower, Understanding hydraulic mounts for improved vehicle noise, vibration and ride qualities, SAE Technical Paper Series 850975, 1985.

[2] A. Geisberger, A. Khajepour, F. Golnaraghi, Non-linear modeling of hydraulic mounts: theory and experiment, *Journal of Sound and Vibration* 249 (2002) 371–397.

[3] J.E. Colgate, C.T. Chang, Y.C. Chiou, W.K. Kiu, L.M. Keer, Modeling of a hydraulic engine mount focusing on response to sinusoidal and composite excitations, *Journal of Sound and Vibration* 184 (1995) 503–528.

[4] J. Christopherson, G.N. Jazar, Optimization of classical hydraulic engine mounts based on RMS method, *Journal of the Shock and Vibration* 12 (12) (2005) 119–147.

[5] R. Singh, G. Kim, P.V. Ravindra, Linear analysis of automotive hydro-mechanical mount with emphasis on decoupler characteristics, *Journal of Sound and Vibration* 158 (1992) 219–243.

[6] G. Kim, R. Singh, A study of passive and adaptive hydraulic engine mount systems with emphasis on non-linear characteristics, *Journal of Sound and Vibration* 179 (1995) 427–453.

[7] G.N. Jazar, M.F. Golnaraghi, Nonlinear modeling of hydraulic mounts: theory and experiment, *Journal of Sound and Vibration* 8 (2002) 87–116.

[8] M.F. Golnaraghi, G.N. Jazar, Development and analysis of a simplified nonlinear model of a hydraulic engine mount, *Journal of Vibration and Control* 7 (2001) 495–526.
[9] H. Adiguna, M. Tiwari, R. Singh, H.E. Tseng, D. Hrovat, Transient response of a hydraulic engine mount, *Journal of Sound and Vibration* 268 (2003) 217–248.
[10] W.B. Shangguan, Z.H. Lu, Modelling of a hydraulic engine mount with fluid-structure interaction finite element analysis, *Journal of Sound and Vibration* 275 (1–2) (2004) 193–221.
[11] A.H. Nayfeh, D. Mook, *Nonlinear Oscillations*, Wiley, New York, 1979.
[12] G.N. Jazar, Stability chart of parametric vibrating systems using energy method, *International Journal of Non-Linear Mechanics* 39 (8) (2004) 1319–1331.